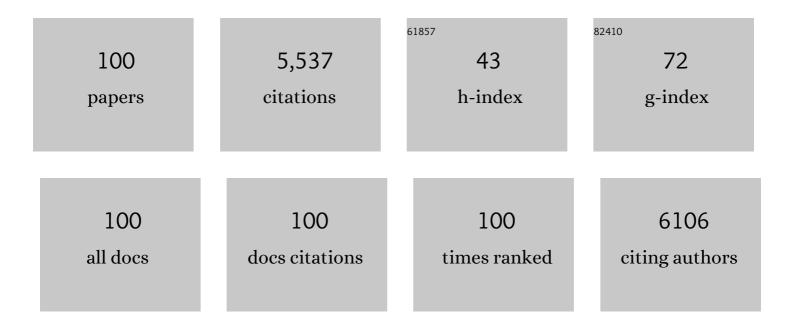
List of Publications by Year in descending order

Source: https://exaly.com/author-pdf/5620740/publications.pdf Version: 2024-02-01



<u> Сыштын Мл</u>

#	Article	IF	CITATIONS
1	Carbon-dot-based ratiometric fluorescent sensor for detecting hydrogen sulfide in aqueous media and inside live cells. Chemical Communications, 2013, 49, 403-405.	2.2	440
2	Real-Time Monitoring of Endogenous Cysteine Levels In Vivo by near-Infrared Turn-on Fluorescent Probe with Large Stokes Shift. Analytical Chemistry, 2018, 90, 1014-1020.	3.2	204
3	Pyrene Derivative Emitting Red or near-Infrared Light with Monomer/Excimer Conversion and Its Application to Ratiometric Detection of Hypochlorite. ACS Applied Materials & Interfaces, 2016, 8, 1511-1519.	4.0	191
4	Carbon dots-based fluorescent probes for sensitive and selective detection of iodide. Mikrochimica Acta, 2013, 180, 453-460.	2.5	160
5	Ratiometric detection and imaging of endogenous hypochlorite in live cells and in vivo achieved by using an aggregation induced emission (AIE)-based nanoprobe. Chemical Communications, 2016, 52, 7288-7291.	2.2	146
6	A two-photon fluorescent sensor revealing drug-induced liver injury via tracking γ-glutamyltranspeptidase (GGT) level inÂvivo. Biomaterials, 2016, 80, 46-56.	5.7	141
7	Nanoaggregate Probe for Breast Cancer Metastasis through Multispectral Optoacoustic Tomography and Aggregationâ€Induced NIRâ€I/II Fluorescence Imaging. Angewandte Chemie - International Edition, 2020, 59, 10111-10121.	7.2	140
8	A highly selective fluorescent nanoprobe based on AIE and ESIPT for imaging hydrogen sulfide in live cells and zebrafish. Materials Chemistry Frontiers, 2017, 1, 838-845.	3.2	132
9	Ratiometric Fluorescent Probe for Alkaline Phosphatase Based on Betaine-Modified Polyethylenimine via Excimer/Monomer Conversion. Analytical Chemistry, 2014, 86, 9873-9879.	3.2	128
10	A fluorescent probe for simultaneous discrimination of GSH and Cys/Hcy in human serum samples via distinctly-separated emissions with independent excitations. Biosensors and Bioelectronics, 2016, 81, 341-348.	5.3	128
11	Activatable probes for diagnosing and positioning liver injury and metastatic tumors by multispectral optoacoustic tomography. Nature Communications, 2018, 9, 3983.	5.8	128
12	A Fluorescence Turnâ€on Sensor for Iodide Based on a Thymine–Hg ^{II} –Thymine Complex. Chemistry - A European Journal, 2011, 17, 14844-14850.	1.7	119
13	Preparation of a Mitochondriaâ€ŧargeted and NOâ€Releasing Nanoplatform and its Enhanced Proâ€Apoptotic Effect on Cancer Cells. Small, 2014, 10, 3750-3760.	5.2	117
14	A ratiometric fluorescent system for carboxylesterase detection with AIE dots as FRET donors. Chemical Communications, 2015, 51, 12791-12794.	2.2	104
15	A PEGylated Fluorescent Turnâ€On Sensor for Detecting Fluoride Ions in Totally Aqueous Media and Its Imaging in Live Cells. Chemistry - A European Journal, 2013, 19, 936-942.	1.7	102
16	Waterâ€Dispersible Fullerene Aggregates as a Targeted Anticancer Prodrug with both Chemo―and Photodynamic Therapeutic Actions. Small, 2013, 9, 613-621.	5.2	97
17	Polymer Micelle with pH-Triggered Hydrophobic–Hydrophilic Transition and De-Cross-Linking Process in the Core and Its Application for Targeted Anticancer Drug Delivery. Biomacromolecules, 2012, 13, 4126-4137.	2.6	95
18	Dual-Targeting Nanosystem for Enhancing Photodynamic Therapy Efficiency. ACS Applied Materials & Interfaces, 2015, 7, 9287-9296.	4.0	92

#	Article	IF	CITATIONS
19	An AIE-based fluorescent test strip for the portable detection of gaseous phosgene. Chemical Communications, 2017, 53, 9813-9816.	2.2	87
20	A fluorescent ratiometric nanosensor for detecting NO in aqueous media and imaging exogenous and endogenous NO in live cells. Journal of Materials Chemistry B, 2013, 1, 4152.	2.9	82
21	Ratiometric fluorescence assay for $\hat{1}^3$ -glutamyltranspeptidase detection based on a single fluorophore via analyte-induced variation of substitution. Chemical Communications, 2014, 50, 3417.	2.2	79
22	A fast-responding fluorescent turn-on sensor for sensitive and selective detection of sulfite anions. Analytical Methods, 2012, 4, 2638.	1.3	78
23	A DT-diaphorase responsive theranostic prodrug for diagnosis, drug release monitoring and therapy. Chemical Communications, 2015, 51, 9567-9570.	2.2	78
24	A Gold Nanocage/Cluster Hybrid Structure for Wholeâ€Body Multispectral Optoacoustic Tomography Imaging, EGFR Inhibitor Delivery, and Photothermal Therapy. Small, 2019, 15, e1900309.	5.2	73
25	A water-soluble and specific BODIPY-based fluorescent probe for hypochlorite detection and cell imaging. Analytical Methods, 2013, 5, 5589.	1.3	71
26	A fluorescent assay for Î ³ -glutamyltranspeptidase via aggregation induced emission and its applications in real samples. Biosensors and Bioelectronics, 2016, 85, 317-323.	5.3	71
27	Hyperbranched Polyester-Based Fluorescent Probe for Histone Deacetylase via Aggregation-Induced Emission. Biomacromolecules, 2013, 14, 4507-4514.	2.6	69
28	Diagnosing Drug-Induced Liver Injury by Multispectral Optoacoustic Tomography and Fluorescence Imaging Using a Leucine-Aminopeptidase-Activated Probe. Analytical Chemistry, 2019, 91, 8085-8092.	3.2	63
29	A H2O2-activatable nanoprobe for diagnosing interstitial cystitis and liver ischemia-reperfusion injury via multispectral optoacoustic tomography and NIR-II fluorescent imaging. Nature Communications, 2021, 12, 6870.	5.8	63
30	Biomarker-activatable probes based on smart AlEgens for fluorescence and optoacoustic imaging. Coordination Chemistry Reviews, 2022, 458, 214438.	9.5	62
31	Handy ratiometric detection of gaseous nerve agents with AIE-fluorophore-based solid test strips. Journal of Materials Chemistry C, 2016, 4, 10105-10110.	2.7	61
32	An Activatable Near-Infrared Chromophore for Multispectral Optoacoustic Imaging of Tumor Hypoxia and for Tumor Inhibition. Theranostics, 2019, 9, 7313-7324.	4.6	60
33	A Turn-On Optoacoustic Probe for Imaging Metformin-Induced Upregulation of Hepatic Hydrogen Sulfide and Subsequent Liver Injury. Theranostics, 2019, 9, 77-89.	4.6	59
34	A ratiometric fluorescent probe for in vivo tracking of alkaline phosphatase level variation resulting from drug-induced organ damage. Journal of Materials Chemistry B, 2015, 3, 1042-1048.	2.9	58
35	A self-immolative prodrug nanosystem capable of releasing a drug and a NIR reporter for inÂvivo imaging and therapy. Biomaterials, 2017, 139, 139-150.	5.7	58
36	Emerging contrast agents for multispectral optoacoustic imaging and their biomedical applications. Chemical Society Reviews, 2021, 50, 7924-7940.	18.7	58

#	Article	IF	CITATIONS
37	Activatable Nanocomposite Probe for Preoperative Location and Intraoperative Navigation for Orthotopic Hepatic Tumor Resection via MSOT and Aggregation-Induced Near-IR-I/II Fluorescence Imaging. Analytical Chemistry, 2020, 92, 9257-9264.	3.2	54
38	A Fluorescent Probe for Early Detection of Melanoma and Its Metastasis by Specifically Imaging Tyrosinase Activity in a Mouse Model. Analytical Chemistry, 2018, 90, 8807-8815.	3.2	53
39	A bioorthogonal nanosystem for imaging and inÂvivo tumor inhibition. Biomaterials, 2017, 138, 57-68.	5.7	49
40	Nanosized diblock copolymer micelles as a scaffold for constructing a ratiometric fluorescent sensor for metal ion detection in aqueous media. Nanotechnology, 2010, 21, 195501.	1.3	48
41	Fluorescent nanoprobe for in-vivo ratiometric imaging of endogenous hydrogen peroxide resulted from drug-induced organ damages. Biosensors and Bioelectronics, 2017, 94, 278-285.	5.3	48
42	A Nanoprobe for Diagnosing and Mapping Lymphatic Metastasis of Tumor Using 3D Multispectral Optoacoustic Tomography Owing to Aggregation/Deaggregation Induced Spectral Change. Advanced Functional Materials, 2019, 29, 1807960.	7.8	46
43	A turn-on fluorescence probe based on aggregation-induced emission for leucine aminopeptidase in living cells and tumor tissue. Analytica Chimica Acta, 2018, 1031, 169-177.	2.6	45
44	A Fluorescent Probe with Aggregationâ€Induced Emission for Detecting Alkaline Phosphatase and Cell Imaging. Chemistry - an Asian Journal, 2019, 14, 802-808.	1.7	45
45	Mesoporous silica particles for selective detection of dopamine with β-cyclodextrin as the selective barricade. Chemical Communications, 2011, 47, 9086.	2.2	43
46	Cell-penetrating poly(disulfide)-based star polymers for simultaneous intracellular delivery of miRNAs and small molecule drugs. Polymer Chemistry, 2017, 8, 4043-4051.	1.9	43
47	A polylysine-based fluorescent probe for sulfite anion detection in aqueous media via analyte-induced charge generation and complexation. Polymer Chemistry, 2013, 4, 5416.	1.9	42
48	Simultaneous Imaging of Endogenous Survivin mRNA and On-Demand Drug Release in Live Cells by Using a Mesoporous Silica Nanoquencher. Small, 2017, 13, 1700569.	5.2	42
49	Tumor Inhibition Achieved by Targeting and Regulating Multiple Key Elements in EGFR Signaling Pathway Using a Selfâ€Assembled Nanoprodrug. Advanced Functional Materials, 2018, 28, 1800692.	7.8	42
50	One-pot fabrication of polymer nanoparticle-based chemosensors for Cu2+ detection in aqueous media. Polymer Chemistry, 2013, 4, 2325.	1.9	41
51	A Nanosystem Capable of Releasing a Photosensitizer Bioprecursor under Twoâ€Photon Irradiation for Photodynamic Therapy. Advanced Science, 2016, 3, 1500254.	5.6	41
52	An AlEgen-based oral-administration nanosystem for detection and therapy of ulcerative colitis via 3D-MSOT/NIR-II fluorescent imaging and inhibiting NLRP3 inflammasome. Biomaterials, 2022, 283, 121468.	5.7	41
53	A ratiometric fluorescent probe for aluminum ions based-on monomer/excimer conversion and its applications to real samples. Talanta, 2016, 151, 8-13.	2.9	39
54	A dopamine-precursor-based nanoprodrug for in-situ drug release and treatment of acute liver failure by inhibiting NLRP3 inflammasome and facilitating liver regeneration. Biomaterials, 2021, 268, 120573.	5.7	39

#	Article	IF	CITATIONS
55	An Activatable Probe with Aggregationâ€Induced Emission for Detecting and Imaging Herbal Medicine Induced Liver Injury with Optoacoustic Imaging and NIRâ€II Fluorescence Imaging. Advanced Healthcare Materials, 2021, 10, e2100867.	3.9	37
56	Oligo(ethylene glycol)-Functionalized Squaraine Fluorophore as a Near-Infrared-Fluorescent Probe for the In Vivo Detection of Diagnostic Enzymes. Analytical Chemistry, 2018, 90, 9359-9365.	3.2	35
57	Nanoaggregate Probe for Breast Cancer Metastasis through Multispectral Optoacoustic Tomography and Aggregationâ€Induced NIRâ€I/II Fluorescence Imaging. Angewandte Chemie, 2020, 132, 10197-10207.	1.6	35
58	A self-immolative and DT-diaphorase-activatable prodrug for drug-release tracking and therapy. Journal of Materials Chemistry B, 2017, 5, 2635-2643.	2.9	33
59	A sequential enzyme-activated and light-triggered pro-prodrug nanosystem for cancer detection and therapy. Journal of Materials Chemistry B, 2018, 6, 2547-2556.	2.9	33
60	A fluorescent probe based on aggregation-induced emission for hydrogen sulfide-specific assaying in food and biological systems. Analyst, The, 2019, 144, 6570-6577.	1.7	33
61	A mitochondrial-targeting and NO-based anticancer nanosystem with enhanced photo-controllability and low dark-toxicity. Journal of Materials Chemistry B, 2015, 3, 4904-4912.	2.9	32
62	A ratiometric fluorescent probe for hyaluronidase detection via hyaluronan-induced formation of red-light emitting excimers. Biosensors and Bioelectronics, 2016, 79, 776-783.	5.3	31
63	Grafting zwitterionic polymer chains onto PEI as a convenient strategy to enhance gene delivery performance. Polymer Chemistry, 2013, 4, 5810.	1.9	30
64	A two-photon-activated prodrug for therapy and drug release monitoring. Journal of Materials Chemistry B, 2017, 5, 7538-7546.	2.9	30
65	Ratiometric sensing of mercury(II) based on a FRET process on silica core-shell nanoparticles acting as vehicles. Mikrochimica Acta, 2013, 180, 845-853.	2.5	29
66	Low molecular weight PEIs modified by hydrazone-based crosslinker and betaine as improved gene carriers. Colloids and Surfaces B: Biointerfaces, 2014, 122, 472-481.	2.5	26
67	A conjugated-polymer-based ratiometric nanoprobe for evaluating in-vivo hepatotoxicity induced by herbal medicine via MSOT imaging. Photoacoustics, 2019, 13, 6-17.	4.4	26
68	An activatable probe for detecting alcoholic liver injury <i>via</i> multispectral optoacoustic tomography and fluorescence imaging. Chemical Communications, 2020, 56, 11102-11105.	2.2	26
69	Activatable fluorescent probe based on aggregation-induced emission for detecting hypoxia-related pathological conditions. Analytica Chimica Acta, 2020, 1125, 152-161.	2.6	26
70	Phase separation in poly(N-isopropyl acrylamide)/water solutions. II. Salt effects on cloud-point curves and gelation. Journal of Polymer Science, Part B: Polymer Physics, 2001, 39, 901-907.	2.4	24
71	Bioorthogonal Nanosystem for Near-Infrared Fluorescence Imaging and Prodrug Activation in Mouse Model. , 2019, 1, 549-557.		24
72	An Activatable Nanoâ€Prodrug for Treating Tyrosineâ€Kinaseâ€Inhibitorâ€Resistant Nonâ€Small Cell Lung Cancer and for Optoacoustic and Fluorescent Imaging. Small, 2020, 16, e2003451.	5.2	24

#	Article	IF	CITATIONS
73	A turn-on probe for detecting antituberculotic drug-induced liver injury in mice <i>via</i> NIR-II fluorescence/optoacoustic imaging. Chemical Communications, 2021, 57, 7842-7845.	2.2	23
74	Aminopeptidase N Activatable Nanoprobe for Tracking Lymphatic Metastasis and Guiding Tumor Resection Surgery via Optoacoustic/NIR-II Fluorescence Dual-Mode Imaging. Analytical Chemistry, 2022, 94, 8449-8457.	3.2	22
75	Tetrazine-Mediated Bioorthogonal System for Prodrug Activation, Photothermal Therapy, and Optoacoustic Imaging. ACS Applied Materials & Interfaces, 2019, 11, 41875-41888.	4.0	21
76	An anthracenecarboximide fluorescent probe for in vitro and in vivo ratiometric imaging of endogenous alpha- <scp>l</scp> -fucosidase for hepatocellular carcinoma diagnosis. Materials Chemistry Frontiers, 2017, 1, 660-667.	3.2	20
77	Targeted anti-cancer prodrug based on carbon nanotube with photodynamic therapeutic effect and pH-triggered drug release. Journal of Nanoparticle Research, 2013, 15, 1.	0.8	19
78	An Unsymmetrical Squaraineâ€Based Activatable Probe for Imaging Lymphatic Metastasis by Responding to Tumor Hypoxia with MSOT and Aggregationâ€Enhanced Fluorescent Imaging. Chemistry - A European Journal, 2019, 25, 16740-16747.	1.7	18
79	Fluorophore-Dapagliflozin Dyad for Detecting Diabetic Liver/Kidney Damages via Fluorescent Imaging and Treating Diabetes via Inhibiting SGLT2. Analytical Chemistry, 2021, 93, 4647-4656.	3.2	18
80	Tetranitrile-anthracene as a probe for fluorescence detection of viscosity in fluid drinks <i>via</i> aggregation-induced emission. Analyst, The, 2020, 145, 844-850.	1.7	17
81	Preparation of Highly Charged, Monodisperse Nanospheres. Macromolecular Chemistry and Physics, 2002, 203, 673-677.	1.1	14
82	A biopolymer-based and inflammation-responsive nanodrug for rheumatoid arthritis treatment <i>via</i> inhibiting JAK-STAT and JNK signalling pathways. Nanoscale, 2020, 12, 23013-23027.	2.8	14
83	Rational design of stable heptamethine cyanines and development of a biomarker-activatable probe for detecting acute lung/kidney injuries <i>via</i> NIR-II fluorescence imaging. Analyst, The, 2022, 147, 410-416.	1.7	13
84	A Targeted Nanosystem for Detection of Inflammatory Diseases via Fluorescent/Optoacoustic Imaging and Therapy via Modulating Nrf2/NFâ€₽B Pathways. Small, 2021, 17, e2102598.	5.2	12
85	Therapeutic Nanosystem Consisting of Singlet-Oxygen-Responsive Prodrug and Photosensitizer Excited by Two-Photon Light. ACS Medicinal Chemistry Letters, 2018, 9, 23-27.	1.3	11
86	Refashioning benzothiadiazole dye as an activatable nanoprobe for biomarker detection with NIR-II fluorescence/optoacoustic imaging. Cell Reports Physical Science, 2022, 3, 100570.	2.8	10
87	An activatable probe for detection and therapy of food-additive-related hepatic injury via NIR-II fluorescence/optoacoustic imaging and biomarker-triggered drug release. Analytica Chimica Acta, 2022, 1208, 339831.	2.6	9
88	AIE fluorophore with enhanced cellular uptake for tracking esterase-activated release of taurine and ROS scavenging. Faraday Discussions, 2017, 196, 335-350.	1.6	8
89	Targeted and activatable nanosystem for fluorescent and optoacoustic imaging of immune-mediated inflammatory diseases and therapy via inhibiting NF-κB/NLRP3 pathways. Bioactive Materials, 2022, 10, 79-92.	8.6	8
90	<scp>Nearâ€Infrared</scp> Fluorescent Nanoprobe for Detecting Hydrogen Peroxide in Inflammation and Ischemic Kidney Injury. Chinese Journal of Chemistry, 2020, 38, 1304-1310.	2.6	8

Sниіzни Wu

#	Article	IF	CITATIONS
91	Modulation of Fluorescence of a Terbium-Complex-Containing Polymer by Gold Nanoparticles through Energy Transfer. Journal of Inorganic and Organometallic Polymers and Materials, 2007, 17, 679-685.	1.9	7
92	Biomarker-responsive nanoprobe with aggregation-induced emission for locating and guiding resection of deep-seated tumors <i>via</i> optoacoustic and NIR fluorescence imaging. Materials Chemistry Frontiers, 2021, 5, 1962-1970.	3.2	7
93	Optical molecular imaging and theranostics in neurological diseases based on aggregation-induced emission luminogens. European Journal of Nuclear Medicine and Molecular Imaging, 2022, 49, 4529-4550.	3.3	7
94	Preparation of colloidal crystals with polyhedral building blocks through post-polymerization. Colloid and Polymer Science, 2004, 282, 651-655.	1.0	6
95	Tunability of Fluorescence Property of a Terbium-Complex-Containing Polymer via Incorporation of a Transition-Metal Complex. Macromolecular Rapid Communications, 2006, 27, 937-942.	2.0	6
96	Thermal reversible gelation during phase separation of poly(N-isopropyl acrylamide)/water solution. Science in China Series B: Chemistry, 2000, 43, 428-434.	0.8	5
97	Synthesis of NQO1-activatable Optoacoustic Probe and Its Imaging of Breast Cancer. Acta Chimica Sinica, 2021, 79, 331.	0.5	4
98	ALP-activated probe for diagnosis of liver injury by multispectral optoacoustic tomography. Methods in Enzymology, 2021, 657, 301-330.	0.4	1
99	Interactions Between Gold Nanoparticles and Polymer Bearing 3-Styryl Thiophene Chromophores. Journal of Inorganic and Organometallic Polymers and Materials, 2008, 18, 463-471.	1.9	Ο
100	A dual-targeting strategy to enhance photodynamic efficacy using a pH-responsive polymeric micelles. Journal of Controlled Release, 2015, 213, e49.	4.8	0